



Shi Jian (Orcid ID: 0000-0002-0703-4612)

Yan Qing (Orcid ID: 0000-0001-5299-7824)

## **Possible modulation of the interannual ENSO-East Asian winter monsoon relationship by the North American ice sheets during the last 21 ka**

**Jian Shi<sup>1</sup>, Qing Yan<sup>2,3</sup>, Yize Yang<sup>1</sup>, and Fang Zhou<sup>4</sup>**

<sup>1</sup>Key Laboratory of Meteorological Disaster, Ministry of Education/Collaborative Innovation Center on Forecast and Evaluation of Meteorological Disasters, Nanjing University of Information Science and Technology, Nanjing, China.

<sup>2</sup>Nansen-Zhu International Research Centre, Institute of Atmospheric Physics, Chinese Academy of Sciences, Beijing, China.

<sup>3</sup>CAS Center for Excellence in Tibetan Plateau Earth Sciences, Chinese Academy of Sciences, Beijing, China.

<sup>4</sup>Climate Change Research Center, Institute of Atmospheric Physics, Chinese Academy of Sciences, Beijing, China.

Corresponding author: Jian Shi ([shij@nuist.edu.cn](mailto:shij@nuist.edu.cn))

### **Key Points:**

- The ENSO–East Asian winter monsoon relationship (EER) is significantly strengthened during the last glacial maximum and early deglaciation
- The strengthened EER is characterized by the poleward shift of ENSO’s influence over the northwest Pacific
- Large North American ice sheets are the ultimate driver of the strengthened EER at that time

This article has been accepted for publication and undergone full peer review but has not been through the copyediting, typesetting, pagination and proofreading process which may lead to differences between this version and the Version of Record. Please cite this article as doi: 10.1029/2020GL089572

## Abstract

Observations have demonstrated an unstable interannual relationship between El Niño/Southern Oscillation (ENSO) and the East Asian winter monsoon (EAWM) in recent decades due to internal variability. However, it remains unclear whether the interannual ENSO-EAWM relationship (EER) may change with long-term external forcings, especially when they vary substantially. The results of a set of transient simulations during the last 21000 years demonstrate the EER is enhanced during the last glacial maximum relative to the Holocene, characterized by a poleward migration of ENSO's signal over the Northwest Pacific. The strengthened EER results from the weakened interannual ENSO-Aleutian Low teleconnection and the northeastward displacement of the climatological Aleutian Low, ultimately forced by the massive North American ice sheets at that time. Our study suggests a changing EER with various external forcings and implies potential uncertainty in applying the present-day ENSO teleconnections during glacials.

## Plain Language Summary

The East Asian winter monsoon (EAWM) exerts significant impacts on the climate over Asia and affects billions of people; thus, a precise EAWM prediction is urgently required. Since the El Niño/South Oscillation (ENSO) provides the majority of skillful predictability, the effect of ENSO on EAWM has received considerable attention. Although recent studies noticed that the ENSO-EAWM relationship (EER) was unstable during recent decades due to the oceanic oscillations, such as the Pacific Decadal Oscillation and Atlantic Multidecadal Oscillation, it remains unclear whether the EER could change with substantially varied external forcings in the future, such as solar insolation, greenhouse gases, meltwater flux, and ice sheets. Using a set of transient simulations during the last 21000 years, we found that the EER is significantly strengthened during the last glacial maximum and early deglaciation relative to the Holocene, attributed to the vast North American ice sheets at that time. Therefore, this study will not only have great significance for the paleoclimate research, which usually applied the present-day ENSO teleconnection to explain past changes in regional climate directly, but also help to project the future EER variation for a better EAWM prediction.

## 1 Introduction

The East Asian winter monsoon (EAWM), one of the most prominent climate systems in the Northern Hemisphere during boreal winter, is characterized by the cold northwesterly winds prevailing along the coast of East Asia (An, 2000; Wang and Chen, 2010; Huang et al., 2012), and producing severe cold surges and heavy snowfall events (Ji et al., 1997; Zhang et al., 1997; Chang et al., 2006). Given its significant impact on weather and climate, sustained efforts have been made to understand the dynamics of and factors influencing the EAWM (Gong et al., 2001; Wu et al., 2002; Yang et al., 2002; Chen et al., 2005; Wang et al., 2010). Notably, on the interannual timescale, the El Niño/Southern Oscillation (ENSO) has a significant inverse relationship with the EAWM (Zhang et al., 1996; Jhun and Lee, 2004; Wang et al., 2000; Wang et al., 2010). During the El Niño (La Niña) winter, the warming (cooling) over the eastern Pacific establishes a favorable (unfavorable) large-scale environment for the air-sea interaction over the western North Pacific, which forms an anomalous anticyclone (cyclone) there and weakens (strengthens) the EAWM (Wang et al., 2000). However, recent studies indicated that the interannual ENSO-EAWM relationship (EER) is unstable in recent decades (Wang and He, 2012; He et al., 2013). For instance, the EER was significant before the 1970s and after the 2000s, while nonsignificant during the 1980s and 1990s, which may be modulated by the Atlantic Multidecadal Oscillations (AMO)

or the Pacific Decadal Oscillation (PDO) (He and Wang, 2013; Wang et al., 2008; Geng et al., 2017; Kim et al., 2014; Kim et al., 2017).

It is of great importance to comprehend the interannual EER behavior and possible drivers to deepen our knowledge of the stability of ENSO's impact on the East Asian climate and thus provide a better future projection. Nevertheless, existing studies have focused on the role of internal variability in the climate system (i.e., the AMO and PDO). The stability of the interannual EER in response to various external forcings remains unclear. In the future, as global temperature rises due to increased greenhouse gas concentrations (Stott, 2000), the Greenland Ice Sheet may completely disappear, changing its topography and releasing excessive meltwater to the ocean (Greve 2000; Huybrechts et al. 2011). Moreover, the winter insolation over the Northern Hemisphere will continuously decrease in the next millennia due to varying orbital parameters (Berger, 1978). These forcings are projected to induce significant climate changes in the long term, while their impact on the EER has not been considered. Therefore, a comprehensive exploration of the EER response to external forcings should be performed.

To obtain better insight into the EER variation under external forcings, we can examine it in a paleoclimate context. During the last 21000 years (21 ka), the Earth's climate experienced remarkable changes due to various external forcings, such as insolation, greenhouse gases, ice sheets, and meltwater fluxes. This period thus provides us with an excellent opportunity to explore how the EER changes with these forcings over a relatively long period. Due to the lack of direct geological evidence for the EER over the last 21 ka, we utilize a set of transient climate simulations to examine the EER changes and associated dynamics.

## 2 Data and Methods

Here, we take advantage of the monthly outputs of a transient climate evolution (hereafter referred to as TraCE) over the last 21 ka based on the Community Climate System Model version 3, forced by varying orbital insolation (ORB), greenhouse gases (GHG), meltwater fluxes (MWF), and continental ice sheets (ICE) (Fig. 1a-c). We also use the decadal-mean seasonal outputs of four sensitivity experiments, driven by the transient ORB, GHGs, MWF, and ICE, respectively, with other forcings and boundary conditions fixed at the start of each simulation. Detailed information about the TraCE can be found in He (2011). Besides, the ENSO intensity is measured by the SST anomaly averaged over the Niño3.4 region ( $5^{\circ}\text{N}$ – $5^{\circ}\text{S}$ ,  $170^{\circ}\text{W}$ – $120^{\circ}\text{W}$ ), and the EAWM index is defined as the regionally averaged meridional winds at 1000 hPa over East Asia ( $10^{\circ}$ – $50^{\circ}\text{N}$ ,  $115^{\circ}$ – $135^{\circ}\text{E}$ ) during boreal winter [December-January-February (DJF)]. Specifically, the EAWM index is multiplied by -1 to ensure that positive values represent northerlies. To obtain the evolution of EER throughout the last 21 ka, we calculate a running correlation between the Niño3.4 and EAWM indices within a 100-year window. Notably, the results of this study are not sensitive to the definition of the EAWM index (Fig. S1).

The TraCE is capable of capturing many aspects of the reconstructed climate since the Last Glacial Maximum (LGM,  $\sim 21$  ka BP), such as the high-latitude temperature (He, 2011; Buizert et al., 2018), East Asian monsoon (Wen et al., 2016; Lu et al., 2019), and ENSO variability (Liu et al., 2014). Beyond that, we evaluate the model's performance in reproducing the observed EER. As shown in Fig. S2, the anomalous anticyclone over the northwest Pacific (NWP-AC)—the critical system connecting El Niño and the weakened EAWM—is restricted to the Philippine Sea. The simulated NWP-AC location is similar to that in modern observations but with much weaker intensity. Liu et al. (2014) also indicated

that the simulated ENSO teleconnection in TraCE is significant and stationary in core regions of ENSO impact, but can be complex where ENSO and local precipitation variability are not highly correlated. Nevertheless, the connection between El Niño and the weakened EAWM is closely related to the NWP-AC's position rather than its strength (He and Wang, 2013; Kim et al., 2017), setting up the foundation for a further investigation of the EER in the past with this model.

### **3 Strengthened interannual EER during the LGM and early last deglaciation**

The interannual EER during the last 21 ka shows significant instability (Fig. 1d). The most striking feature is that the EER is much stronger during the LGM and the early last deglaciation, relative to the Holocene. Besides, the weakening of the EER from the LGM is superposed by the ever-present centennial oscillations. As there is no centennial variability in the external forcings applied in the TraCE (Fig. 1a–c), a Monte-Carlo simulation suggests that the ~400-year fluctuation may come from the internal climate variability, while the shorter oscillations are possibly induced by the running correlation method (Fig. S3). We further examine the changes in the ENSO-EAWM linkage between a strong (LGM, ~21-19 ka BP) and weak [late Holocene (LH), 2-0 ka BP] EER period. Since the impacts of ENSO's cold and warm phases largely mirror each other (Wang et al., 2000), the following discussions focus on the warm phase (i.e., the El Niño). Generally, the NWP-AC is vital to the connection of El Niño and weakened EAWM during the LGM and LH (Fig. 2a and 2c), while their meridional positions are distinct. During the LH, the NWP-AC is located over the Philippine Sea; thus, its influence is more limited over tropical and subtropical East Asia, which mainly weakens the low-latitude EAWM. However, during the LGM, when El Niño occurs, the tropical NWP-AC diminishes, and its center tends to be located over the subtropical northwest Pacific. This meridional migration of the NWP-AC induces a more northward extension of the anomalous southerly along the East Asian coast and hence a more substantial reduction in the extratropical EAWM, intensifying the EER.

The meridional shift of ENSO's impact over the western Pacific is also evident in the sea level pressure (SLP) field. During the LH, the El Niño-regressed SLP over the tropical Pacific manifests a negative Walker circulation pattern, decreasing and increasing over the east and west, respectively (Fig. 2b). During the LGM, however, the anomalous high pressure over the western Pacific moves to the Kuroshio Extension region, indicating a northward shift in the subsidence of the anomalous Walker circulation and corresponding to the suppressed convection in that region (Fig. 2d). Moreover, during the LH, El Niño induces an SLP reduction over the northern and northeast Pacific, implying an eastward retreated but generally deepened Aleutian Low (AL) via the Pacific-North American (PNA) teleconnection (Ropelewski et al., 1986; Leathers et al., 1991). Such an intensified AL could impede the development of El Niño-related NWP-AC in higher latitudes (He and Wang, 2013). Nevertheless, El Niño's influence on the AL weakens during the LGM; therefore, the AL could no longer hamper the NWP-AC from moving northward and hence the poleward development of ENSO's influence over the western Pacific, resulting in a stronger EER.

### **4 Possible modulation by the climate background and external forcings**

Previous studies indicated that the internal decadal variabilities of the climate system, such as the PDO and AMO, could affect the interannual EER through changing the climate background over the Pacific (Wang et al., 2008; He and Wang, 2013; Kim et al., 2017). Here, inspired by these findings, we intend to determine whether the distinct EERs between the LGM and LH are related to their external-forced background differences on the millennial timescale. Figure 3a shows the climatological SLP differences between these two periods. It

is noted that SLP decreases globally in the LGM due to an icy climate at that time. Thus, the SLP differences are calculated after removing its zonal mean for a better representation of the atmospheric activity centers. The climatological SLP during the LH (Fig. 3a) exhibits high- and low-pressure systems (namely, the Siberian high and AL) located over Asia and the northern Pacific, respectively. The climatological AL center is located at approximately 180°E and covers the whole middle-latitude North Pacific, which may lead to the occurrence of the dominant extratropical atmospheric variability over the North Pacific, interrupting the EAWM variability associated with ENSO (Wang et al., 2008). Nevertheless, during the LGM, relative to the LH, the SLP decreases dramatically over the Northeast Pacific and increases over the East Asian coast (Fig. 3a). This dipole anomalous pressure pattern implies a northeastward shifted climatological AL, making the dominant extratropical atmospheric variability move away from East Asia, and creating a stronger EER. To specify our inference, we define an AL location (ALL) index as the regionally averaged SLP difference between the Northeast Pacific and Northwest Pacific based on Fig. 3a, and compare the evolution of the climatological AL location with EER during the last 21 ka. It is clear that the AL experiences an abrupt southwestward shift after 13 ka BP, corresponding to the significantly weakened EER (Fig. 3b). This result implies that the climatological AL location may be a dominant factor for the interannual EER since the LGM. It is noted that the change of EER before and after 14 ka BP is not as abrupt as that of the climatological AL movement, which could result from the strong internal variability of EER.

The last question is what external forcing the changed EER could be attributed to. As the EER in the sensitivity experiments is unavailable due to the lack of annually resolved outputs, we focus on the reason for the climatological AL shift to investigate the EER change indirectly. Figure 3c shows the ALL evolution during the last 21 ka in individual sensitivity experiments, indicating that the ice sheets changes dominate the varying ALL in the TraCE. In particular, in the ICE experiment, the ALL is relatively low from 19-16 ka BP, acutely rises from 16-13 ka BP, during which period most of the Cordilleran Ice Sheet disappeared and Laurentide Ice Sheet rapidly lowered (Fig. 1c and 4a), and remains at the LH level throughout the Holocene. Therefore, we speculate that the massive North American ice sheets are the main factor accounting for the northeastward displacement of the climatological AL or the strengthened EER during the LGM and early deglaciation.

The possible dynamical mechanisms may be as follows. When large North American ice sheets exist, the low-level westerlies over the North Pacific strengthen in the south of its axis and weaken in the north (Fig. 4b), implying an equatorward migration of the low-level jet stream. On the one hand, as the mid-latitude westerlies shift southward, the subpolar gyre strengthens in its southern edge. Consequently, the sea ice is transported anomalously westward in the high-latitude through wind-driven processes (Fig. S4), thus not conducive to sea ice expansion in the eastern part of the North Pacific (Zhu et al., 2014; Lu et al., 2016). This leads to strong local warming through the sea ice albedo positive feedback and hence lower pressure. On the other hand, the southward shifted westerlies inhibit the North Pacific Current, lowering the SSTs over the Kuroshio Extension region, hence creating higher pressure (Fig. 4c–d). Consequently, the northeastern part of the climatological AL intensifies, while the southwestern part weakens, corresponding to a northeastward movement.

In addition, the ALL change is insensitive to other external forcings except for the meltwater discharge, which contributes a small part of the AL movement in certain millennia (i.e., ~15 ka BP). When freshwater discharges into the North Atlantic, the Atlantic dramatically cools in response to an AMOC weakening. The Atlantic cooling and it triggered tropical Pacific cooling then influence the North Pacific through the barotropic Rossby waves (Trenberth et al. 1998; Alexander et al. 2002; Deser and Phillips 2006), enhancing the AL

mostly in its eastern Part (Okumura et al., 2009) and shifting the AL. Nevertheless, the ALL response to meltwater discharge is not well reflected in the EER, which may be obscured by the strong internal fluctuations of EER.

## 5 Conclusion and Discussion

Based on a set of transient climate simulations, we investigate the stability of EER during the last 21 ka and its possible relationship with the climate background and external forcings. The modeled EER is much stronger during the LGM and early last deglaciation relative to the Holocene, confirming a varied ENSO teleconnection from another perspective (Liu et al., 2014). Specifically, the El Niño-induced NWP-AC, generally located over the tropical region during the LH, moves to the subtropical region during the LGM and shifts the associated anomalous southerlies to a higher latitude along the East Asian coast, resulting in a much weaker EAWM. The EAWM response related to La Niña also weakens from the LGM to present, implying that ENSO's impact on the EAWM reduced in both El Niño and La Niña conditions, although their responses are asymmetric (Fig. S5).

The meridional migration of ENSO signals over the western Pacific may be attributed to its varied impact on the AL on the interannual timescale. During the LH, El Niño leads to an overall intensification of the AL, inhibiting the poleward development of the NWP-AC. Nevertheless, during the LGM, El Niño tends to cause an eastward displacement of the AL, reducing its influence over the extratropical northwest Pacific, thus allowing the NWP-AC to develop further northward. Furthermore, we find that the enhanced EER may be relevant to the northeastward shift of the climatological AL during the LGM and early last deglaciation, which is ultimately driven by the large North American ice sheets.

Our inferences are based on numerical simulations, and hence, uncertainties are inevitable. First, the TraCE largely underestimates the intensity of the ENSO-EAWM relationship, which makes our conclusion less robust. As this model performs well in reproducing the NWP-AC's location, we also investigate the variation of its center during the last 21 ka. It shows that NWP-AC's center experiences an evident shift: locating over 20°-30°N before 13 ka BP but over 5°-20°N afterward (Fig. S6). Such a meridional movement of NWP-AC is consistent with the EER change, implying the systematic underestimation of the ENSO teleconnection has little impact on our conclusion. Second, as the EER is predominant at the interannual timescale, the reconstruction of the EER is hampered by the scarcity of ENSO and EAWM proxies with an adequate temporal resolution, making a direct model-data comparison difficult. Third, we focus on the external forcings causing EER changes; however, the internal variability is nonnegligible (Fig. 1d). For example, the EER changes between the LGM and present-day do not show a consistent sign among the Coupled Model Intercomparison Project (CMIP5) models. One important reason is that most public CMIP5 LGM simulations only have a time span of 100 or 200 years, during which the EER is more likely an internal variability consequence. In this sense, long-term integrated transient simulations, e.g., those spanning the last 21 ka, are required to emphasize the influence of external forcings on the EER without being obscured by its internal variability. Admittedly, such long-term integrated simulations are so rare that we use only one in this study, which makes our conclusions partly model-dependent.

Nevertheless, the background climate changes associated with the interannual EER variation in this transient simulation can be qualitatively compared with the reconstructions and multi-model equilibrium simulation results. Proxies in western North America present an anomalous dipole precipitation/humidity pattern during the LGM, with wetter and drier conditions in the southwest and near the ice sheet, respectively (Thompson and Anderson,

2000; Lyle et al., 2012; Oster et al., 2015). This suggests a southward displacement of the North Pacific lower-level subtropical westerly jet stream, which is reproduced in all the LGM simulations of the fifth phase of the CMIP5 (Wang et al., 2018). Moreover, the CMIP simulations consistently indicated a distorted PNA teleconnection during the LGM (Hu et al., 2019), confirming a weakened connection between the tropical (i.e., ENSO) and North Pacific (i.e., AL) climate variability as simulated by the TraCE. More importantly, these proxy and modeling studies highlighted the crucial role of the North American ice sheets, strongly supporting an ice sheet-induced enhancement of the EER during the LGM.

Additionally, the mechanisms of the EER changes inferred from the transient simulation are comparable to those of the modern observational studies, though over a more extended period. For instance, the TraCE implies that the interannual EER changes in the opposite direction to the ENSO-AL relationship during the last 21 ka (Fig. S7), consistent with the observed results during recent decades (Wang and He, 2012; He and Wang, 2013). He and Wang (2013) also found that the anomalous anticyclone could develop over the Kuroshio Extension and the Pacific-East Asia teleconnection (Wang et al., 2000) could be well established only when the anomalous subsidence of the Walker circulation shifted northward. Furthermore, the EER was strengthened when the dominant atmospheric variability retreated from East Asia (i.e., during the negative phase of the PDO; Wang et al., 2008).

Ultimately, we conclude that there was very likely a strengthened relationship between the ENSO and EAWM during the LGM than the present-day using a transient simulation, highlighting the possible modulation of ice sheets on the internal interaction of the climate system. In this sense, we should be more cautious in applying the present-day teleconnections to explain regional climate changes in the past, particularly during glacial periods. Besides, as GHGs, orbital insolation and meltwater exert little impact on the EER, and the North American ice sheet has already completely disappeared, the future EER may be mainly regulated by internal climate variability, fluctuating around the present-day level, rather than influenced by various external forcings.

## Acknowledge

We thank the TraCE-21ka group for sharing their model output via the Earth System Grid of the National Center for Atmospheric Research. The model data are available at <https://www.earthsystemgrid.org/project/trace.html>. This study is supported by the National Key Research and Development Program of China (Grant 2016YFA0600703), the Startup Foundation for Introducing Talent of NUIST (Grant No. 2017r105), and the Strategic Priority Research Program of the Chinese Academy of Sciences (XDA20070103).

## References

- An, Z. (2000). The history and variability of the East Asian paleomonsoon climate. *Quaternary Science Reviews*, 19(1-5), 171-187.
- Berger, A. (1978). Long-term variations of daily insolation and Quaternary climatic changes. *Journal of the atmospheric sciences*, 35(12), 2362-2367.
- Buizert, C., Keisling, B. A., Box, J. E., He, F., Carlson, A. E., Sinclair, G., & DeConto, R. M. (2018). Greenland-Wide Seasonal Temperatures During the Last Deglaciation. *Geophysical Research Letters*, 45(4), 1905-1914.
- Chang, C. P., Wang, Z., & Hendon, H. (2006). The Asian winter monsoon. In *The Asian Monsoon* (pp. 89-127). Springer, Berlin, Heidelberg.

- Chen, W., Yang, S., & Huang, R. H. (2005). Relationship between stationary planetary wave activity and the East Asian winter monsoon. *Journal of Geophysical Research: Atmospheres*, 110(D14).
- Geng, X., Zhang, W., Stuecker, M. F., Liu, P., Jin, F. F., & Tan, G. (2017). Decadal modulation of the ENSO–East Asian winter monsoon relationship by the Atlantic Multidecadal Oscillation. *Climate Dynamics*, 49(7-8), 2531-2544.
- Gong, D. Y., Wang, S. W., & Zhu, J. H. (2001). East Asian winter monsoon and Arctic oscillation. *Geophysical Research Letters*, 28(10), 2073-2076.
- Greve, R. (2000). On the response of the Greenland ice sheet to greenhouse climate change. *Climatic Change*, 46(3), 289-303.
- He, F. (2011) Simulating transient climate evolution of the last deglaciation with CCSM3. *Ph.D. thesis*, University of Wisconsin Madison, 171 pp., [http://www.cgd.ucar.edu/ccr/TraCE/doc/He\\_PhD\\_dissertation\\_UW\\_2011.pdf](http://www.cgd.ucar.edu/ccr/TraCE/doc/He_PhD_dissertation_UW_2011.pdf).
- He, S., & Wang, H. (2013). Oscillating relationship between the East Asian winter monsoon and ENSO. *Journal of Climate*, 26(24), 9819-9838.
- He, S., Wang, H., & Liu, J. (2013). Changes in the relationship between ENSO and Asia–Pacific midlatitude winter atmospheric circulation. *Journal of Climate*, 26(10), 3377-3393.
- Hu, Y., Xia, Y., Liu, Z., Wang, Y., Lu, Z., & Wang, T. (2019). Distorted Pacific-North American Teleconnection at the Last Glacial Maximum. *Climate of the Past Discussions*. 1-24. 10.5194/cp-2019-92.
- Huang, R., Chen, J., Wang, L., & Lin, Z. (2012). Characteristics, processes, and causes of the spatio-temporal variabilities of the East Asian monsoon system. *Advances in Atmospheric Sciences*, 29(5), 910-942.
- Huybrechts, P., Goelzer, H., Janssens, I., Driesschaert, E., Fichefet, T., Goosse, H., & Loutre, M. F. (2011). Response of the Greenland and Antarctic ice sheets to multi-millennial greenhouse warming in the Earth system model of intermediate complexity LOVECLIM. *Surveys in Geophysics*, 32(4-5), 397-416.
- Jhun, J. G., & Lee, E. J. (2004). A new East Asian winter monsoon index and associated characteristics of the winter monsoon. *Journal of Climate*, 17(4), 711-726.
- Ji, L., Sun, S., Arpe, K., & Bengtsson, L. (1997). Model study on the interannual variability of Asian winter monsoon and its influence. *Advances in Atmospheric Sciences*, 14(1), 1-22.
- Kim, J. W., An, S. I., Jun, S. Y., Park, H. J., & Yeh, S. W. (2017). ENSO and East Asian winter monsoon relationship modulation associated with the anomalous northwest Pacific anticyclone. *Climate Dynamics*, 49(4), 1157-1179.
- Kim, J. W., Yeh, S. W., & Chang, E. C. (2014). Combined effect of El Niño–Southern Oscillation and Pacific decadal oscillation on the East Asian winter monsoon. *Climate dynamics*, 42(3-4), 957-971.
- Leathers, D. J., Yarnal, B., & Palecki, M. A. (1991). The Pacific/North American teleconnection pattern and United States climate. Part I: Regional temperature and precipitation associations. *Journal of Climate*, 4(5), 517-528.

- Liu, Z., Lu, Z., Wen, X., Otto-Bliesner, B. L., Timmermann, A., & Cobb, K. M. (2014). Evolution and forcing mechanisms of El Niño over the past 21,000 years. *Nature*, 515(7528), 550.
- Lu, F., Ma, C., Zhu, C., Lu, H., Zhang, X., Huang, K., ... & Zhang, W. (2019). Variability of East Asian summer monsoon precipitation during the Holocene and possible forcing mechanisms. *Climate dynamics*, 52(1-2), 969-989.
- Lu, Z., Liu, Z., & Zhu, J. (2016). Abrupt intensification of ENSO forced by deglacial ice sheet retreat in CCSM3. *Climate Dynamics*, 46, 1877–1891.
- Lyle, M., Heusser, L., Ravelo, C., Yamamoto, M., Barron, J., Diffenbaugh, N. S., ... & Andreasen, D. (2012). Out of the tropics: the Pacific, Great Basin Lakes, and Late Pleistocene water cycle in the western United States. *Science*, 337(6102), 1629-1633.
- Oster, J. L., Ibarra, D. E., Winnick, M. J., & Maher, K. (2015). Steering of westerly storms over western North America at the Last Glacial Maximum. *Nature Geoscience*, 8(3), 201.
- Ropelewski, C. F., & Halpert, M. S. (1986). North American precipitation and temperature patterns associated with the El Niño/Southern Oscillation (ENSO). *Monthly Weather Review*, 114(12), 2352-2362.
- Stott, P. A., Tett, S. F. B., Jones, G. S., Allen, M. R., Mitchell, J. F. B., & Jenkins, G. J. (2000). External control of 20th century temperature by natural and anthropogenic forcings. *Science*, 290(5499), 2133-2137.
- Thompson, R. S., & Anderson, K. H. (2000). Biomes of western North America at 18,000, 6000 and 0 14C yr BP reconstructed from pollen and packrat midden data. *Journal of Biogeography*, 27(3), 555-584.
- Wang, B., Wu, R., & Fu, X. (2000). Pacific–East Asian teleconnection: how does ENSO affect East Asian climate?. *Journal of Climate*, 13(9), 1517-1536.
- Wang, B., Wu, Z., Chang, C. P., Liu, J., Li, J., & Zhou, T. (2010). Another look at interannual-to-interdecadal variations of the East Asian winter monsoon: The northern and southern temperature modes. *Journal of Climate*, 23(6), 1495-1512.
- Wang, H., & He, S. (2012). Weakening relationship between East Asian winter monsoon and ENSO after mid-1970s. *Chinese Science Bulletin*, 57(27), 3535-3540.
- Wang, L., & Chen, W. (2010). How well do existing indices measure the strength of the East Asian winter monsoon?. *Advances in Atmospheric Sciences*, 27(4), 855-870.
- Wang, L., Chen, W., & Huang, R. (2008). Interdecadal modulation of PDO on the impact of ENSO on the East Asian winter monsoon. *Geophysical Research Letters*, 35(20).
- Wang, N., Jiang, D., & Lang, X. (2018). Northern westerlies during the Last Glacial Maximum: Results from CMIP5 simulations. *Journal of Climate*, 31(3), 1135-1153.
- Wen, X., Liu, Z., Wang, S., Cheng, J., & Zhu, J. (2016). Correlation and anti-correlation of the East Asian summer and winter monsoons during the last 21,000 years. *Nature communications*, 7, 11999.
- Wu, B., & Wang, J. (2002). Winter Arctic oscillation, Siberian high and East Asian winter monsoon. *Geophysical research letters*, 29(19), 3-1.

Yang, S., Lau, K. M., & Kim, K. M. (2002). Variations of the East Asian jet stream and Asian–Pacific–American winter climate anomalies. *Journal of Climate*, 15(3), 306-325.

Zhang, R., Sumi, A., & Kimoto, M. (1996). Impact of El Niño on the east Asian monsoon. *Journal of the Meteorological Society of Japan. Ser. II*, 74(1), 49-62.

Zhang, Y., Sperber, K. R., & Boyle, J. S. (1997). Climatology and interannual variation of the East Asian winter monsoon: Results from the 1979–95 NCEP/NCAR reanalysis. *Monthly Weather Review*, 125(10), 2605-2619.

Zhu, J., Liu, Z., Zhang, X., Eisenman, I., & Liu, W. (2014). Linear weakening of the AMOC in response to receding glacial ice sheets in CCSM3. *Geophysical Research Letters*, 41, 6252–6258.

Accepted Article

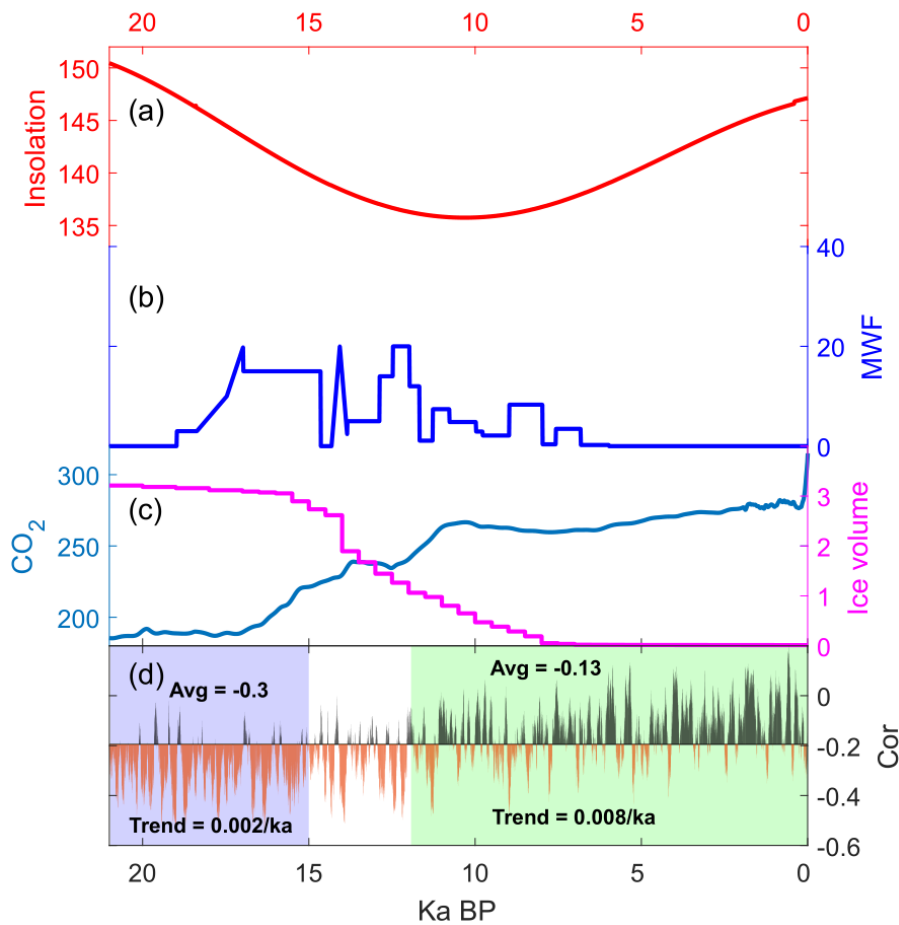


**Figure 1.** Evolution of external forcings and EER during the last 21 ka. (a) DJF insolation at 45°N (in  $W/m^2$ ). (b) meltwater fluxes in the Northern Hemisphere (in meters of global sea level rise per 1000 years). (c) CO<sub>2</sub> concentration (in ppm) and North American Ice volume (in  $10^7 km^3$ ). (d) 100-year running correlation between the DJF Niño3.4 and EAWM index in the TraCE simulation. Correlation coefficients passing the 95% significance test are shaded in orange in (d). The purple and green vertical panels in (d) represent 21-15 and 12-0 ka BP, respectively, with the average (upper) and linear trends (lower) of EERs during these two periods.

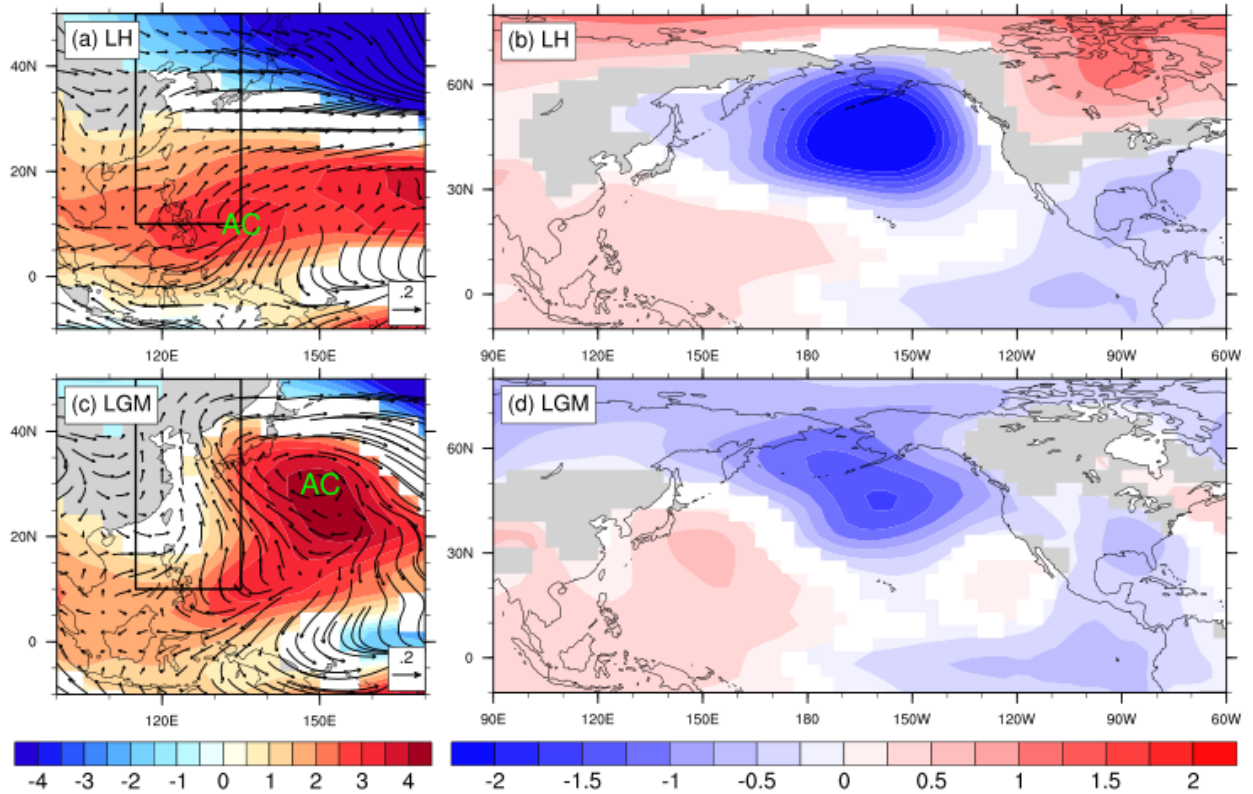


**Figure 2.** Regressed horizontal winds (vectors, in m/s) and stream function (shading, in  $10^5$   $m^2/s$ ) anomalies at 1000 hPa (a, c) and SLP anomalies (in hPa) (b, d) with respect to the Niño3.4 index during the LH (a, b) and LGM (c, d). In (a, c), the rectangles denote the regions for calculating the EAWM index, and “AC” denotes the center of El Niño-induced anticyclone. Only the stream function and SLP anomalies significant at the 95% level are shown.

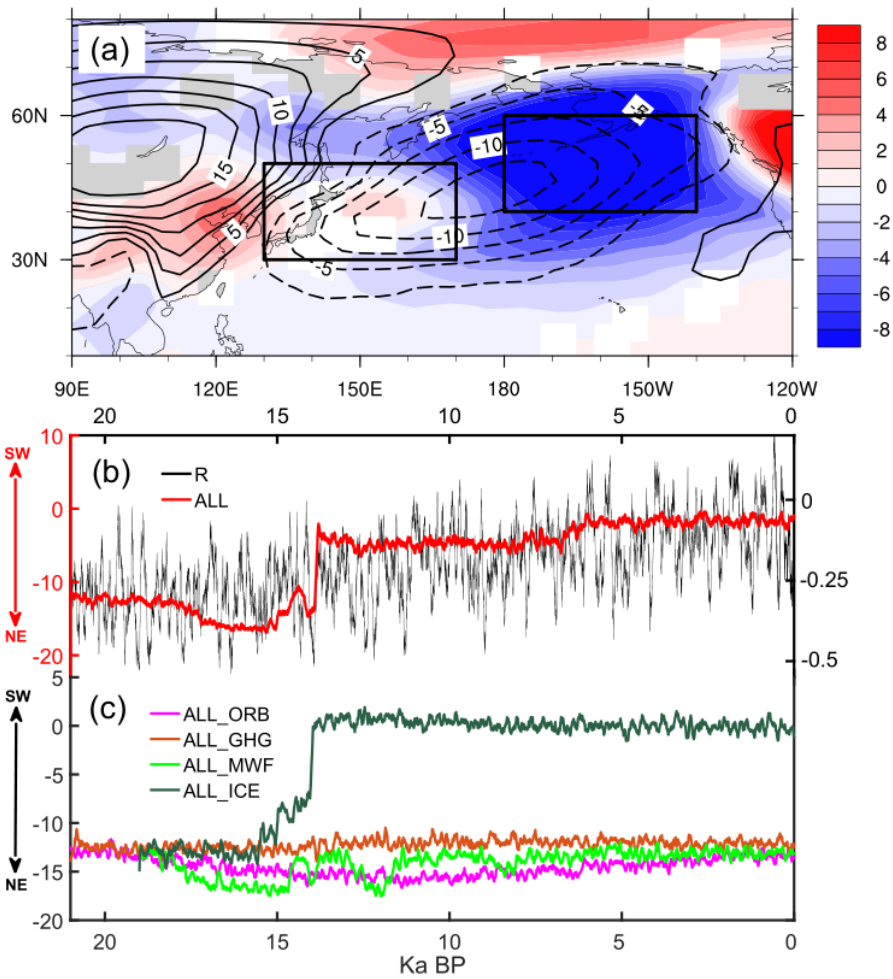


**Figure 3.** (a) Differences in the climatological SLP (shadings, in hPa) between the LGM and LH, and the climatological SLP during the LH (contours, in hPa). (b) 100-year running correlation between the Niño3.4 and EAWM index (black), and ALL index (red, in hPa) in the TraCE during the last 21 ka. (c) ALL in four corresponding sensitivity experiments (in hPa). The ALL index is defined as the SLP difference between  $40^{\circ}$ – $60^{\circ}$ N,  $180^{\circ}$ E– $140^{\circ}$ W and  $30^{\circ}$ – $45^{\circ}$ N,  $130^{\circ}$ – $160^{\circ}$ E, indicated as rectangles in (a). Only the differences significant at the 95% level are shown. “SW” and “NE” denote the southwestward and northeastward displacement of climatological AL, respectively.

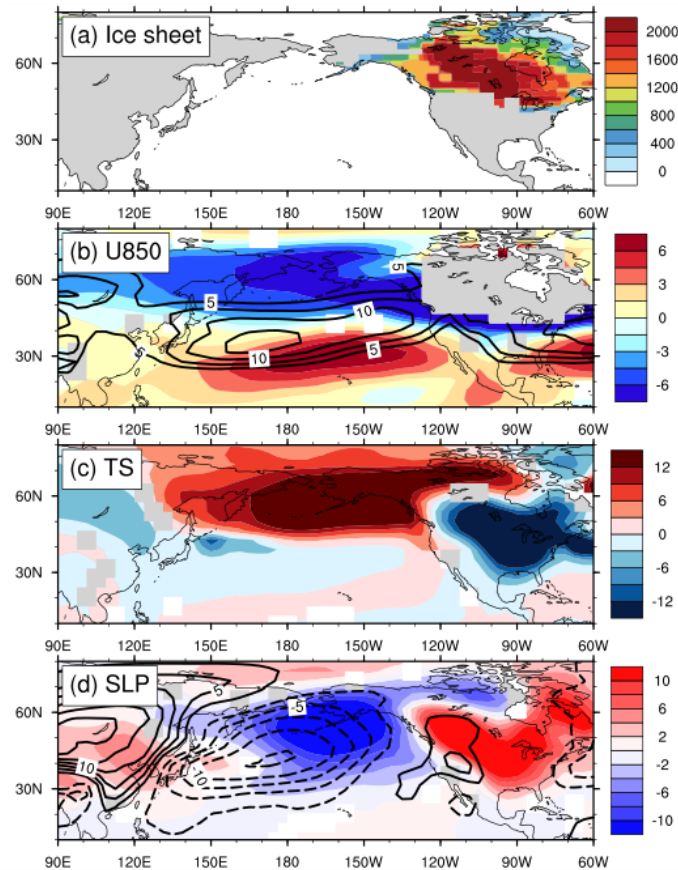


**Figure 4.** The difference in (a) ice sheet thickness (in m), (b) zonal winds at 850 hPa (shadings, in m/s), (c) surface temperature (in K) and (d) SLP (shadings, in hPa) between 19–17 and 2–0 ka BP in the ICE experiment. Contours in (b) and (d) denote the climatological 850 hPa zonal winds (in m/s) and SLP (in hPa) during the LH, respectively. Areas with an elevation below 1500m are masked in (b). Only the differences significant at the 95% level are shown in (b–d).